PRESSURE DROP PREDICTIONS USING *CODE_SATURNE* IN NESTOR CFD BENCHMARK

Benhamadouche S.
EDF R&D, Fluids Mechanics, Energy and Environment Department
6, Quai Watier, 78401 Chatou, France
sofiane.benhamadouche@edf.fr

ABSTRACT

The following study has been partly carried out in the framework of a Round Robin Exercise organized by EPRI in which different CFD results have been compared to high fidelity fuel rod bundle NESTOR Experimental Data (CEA-EDF-EPRI) carried out for PWR configurations. Two types of grids, a simple (SSG) and a complex (MVG) one, have been studied at a Reynolds number around 100000. The present work focuses on the prediction of the pressure drop for the two grids.
EDF in-house and open source CFD tool *Code_Saturne* has been used. Both a first and a second moment closure RANS turbulence model have been utilized. Two wall functions have also been tested.
The effect of the turbulence model is, for the pressure drop prediction, negligible compared to the influence of the wall function. The standard wall function using one friction velocity scale, although not suitable in other configurations, gives the best results.
A systematic underestimation of the pressure drop is obtained for the SSG (around 15% for the best results) even with the best numerical options, usable as the mesh is fully conformal and hexahedral. A systematic underestimation is also observed for the MVG (around 15% error) but with deteriorated numerical options (a steady algorithm and a least square method for computing the gradients) forced by the mesh complexity with alternating SSGs and MVGs (the mesh is fully hexahedral by parts and either a conformal joining using tets/pyramids or a non-conformal joining are used to link SSG and MVG meshes).
Additional tests have been carried out with just one MVG and allowed us to test the effect of the time scheme and the gradient computation as the mesh wall totally conformal and hexahedral. The use of an unsteady algorithm combined to a Gauss implicit gradient computation gave very satisfactory results.

KEYWORDS
CFD, fuel assembly, PWR, pressure drop, NESTOR experimental data

1 INTRODUCTION

The pressure drop coefficients through mixing grids or along bare bundles are mandatory data to be used in coarse approaches which model the whole core of a nuclear vessel. It is therefore interesting to see whether CFD is able to predict such coefficients.

The present study has been partly carried out in the framework of EPRI Round Robin benchmark exercise which used CEA-EDF-EPRI NESTOR experimental data (Bergeron et al. [3]). More details about this benchmark are available in Wells and Hassan [8].

The work presented herein mainly aims at testing the ability of RANS (Reynolds Averaged Navier Stokes) approaches to predict the pressure drop through simple support and complex mixing grids. CFD results are compared to experimental data obtained on a 5x5 PWR bundle sub-assembly geometry during NESTOR project, and more precisely from hydraulic isothermal tests on the EDF-CHATOU MANIVEL

loop for the characterization of friction and/or grid pressure loss, and determination of axial velocity field by Laser-Doppler Velocimetry (LDV) in single-phase flow. Two grids have been tested, a Simple Support Grid (named SSG hereafter) and a Mixing Vane Grid (name complex grid or MVG hereafter).

After the description of the two test-cases, the numerical approach utilized in the present work is detailed. Then, CFD pressure drop results for the two configurations are compared to experimental data. After that, a sensitivity study to two numerical parameters is performed using one MVG. Finally, conclusions are drawn on the ability of CFD to predict pressure drop coefficients for the flow through PWR fuel assemblies.

2 TEST CASES

Two configurations have been studied, the first one with only SSGs (see figure 1), called SSG configuration hereafter, and the second one with alternating SSGs and MVGs (see figure 2), called the MVG configuration hereafter. The bundle is a typical 5x5 one of a PWR (the number of tubes in figures 1 and 2 doesn't represent the real number). The spacing between the center of the peripheral tubes and the wall (casing) is equal to 7.85 mm. The spans have a length equal to 279 mm (a span is defined as the distance between the ends of two successive grids). The experimental domain including the fuel assembly is almost totally represented in the SSG and MVG configurations (see figures 1 and 2). One can notice that there is no SSG between the second and the third MVG in the MVG configuration.

The Reynolds number based on the bulk velocity, the hydraulic diameter and the kinematic viscosity is around 100000 (equal to 96000 and 100000 in the SSG and MVG configurations, respectively).

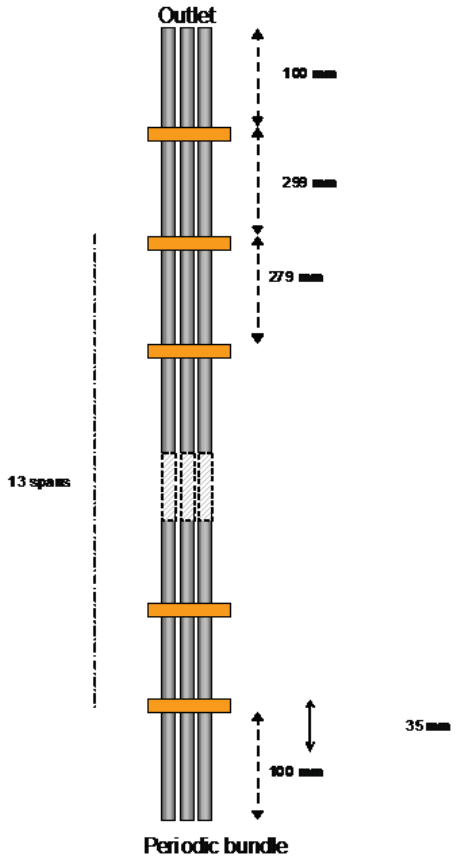

Figure 1 : Computational domain, SSG configuration.

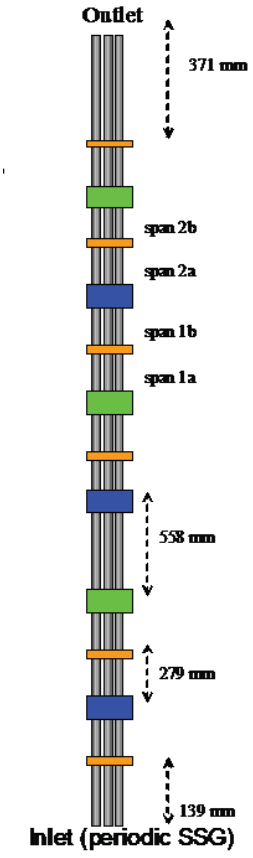

Figure 2 : Computational domain, MVG configuration.

3 NUMERICAL APPROACH

3.1 Mesh Generation

All the elementary (for each grid) meshes have been created with *ICEM CFD using* the blocking method. For more details about the geometrical characteristics of the support and mixing grids, see [8].

The SSG mesh (see figure 3) is fully hexahedral and contains 7 million cells (the height of the grid is 8 mm and the bare bundle length meshed on both sides of the grid is equal to 29,7 mm). The mesh refinement in the stream-wise direction just upstream or downstream the grid is equal to 0.5 mm.

The MVG grid (see figure 4) is also fully hexahedral and contains 5.7 million cells (the height of the grid is 38 mm and the bare bundle length meshed on both sides of the grid is equal to 29,7 mm). The mesh refinement in the stream-wise direction is of the same order as the one used for the SSG. The MVG mesh is coarser than the SSG one due to the present approach using the blocking method (fully hexahedral mesh) and the complexity of the geometry.

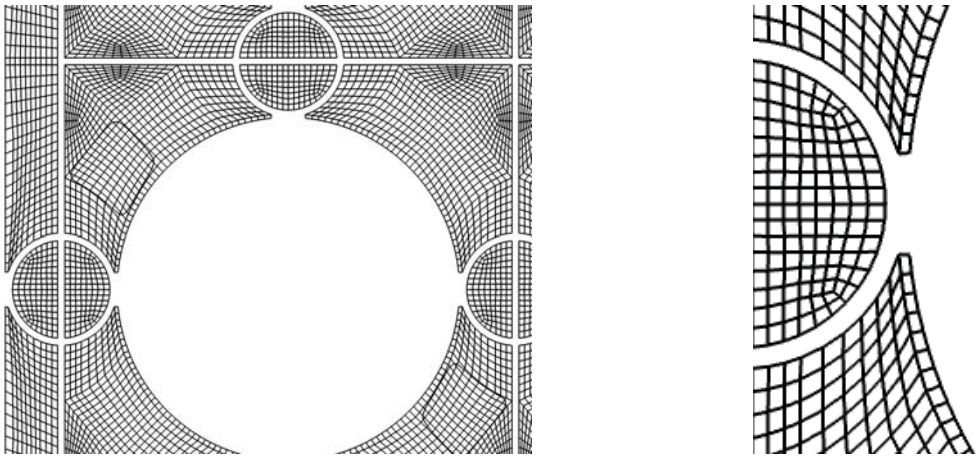

Figure 3 : Left : mesh cut in the SSG, right : zoom around the dimples (simplified contact zone)

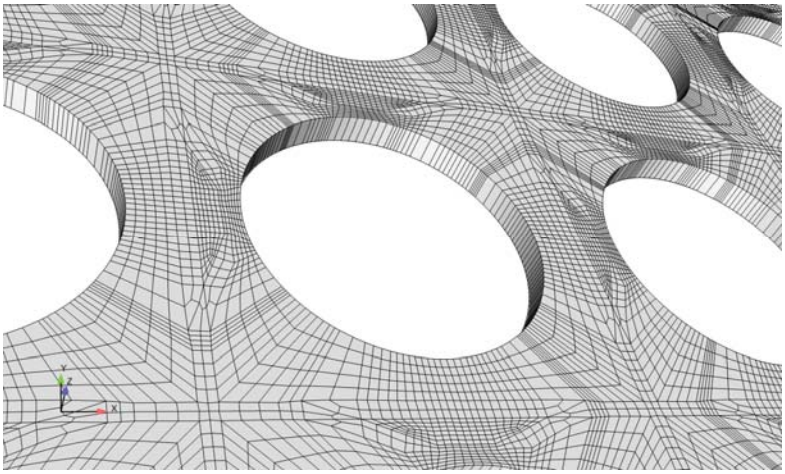

Figure 4 : Mesh cut in the MVG bundle

In the MVG configuration, the SSG and MVG meshes have to be joined. As their topologies are different, it is very difficult, but apparently not impossible (Capone [4]), to join the two meshes in a conformal wayt using only hexahedral cells. Two methods are tested in the present work:

- A conformal joining using pyramids/tetras (see figure 5),
- A non-conformal joining using basically hexahedral elements but formed by more than 6 faces (polyhedral approach, see figure 6).

The first method introduces much more cells and faces than the first one (which actually does not change the number of computational cells). It also leads to arbitrary refinements close to the walls.

The final SSG, MVG with a conformal joining and MVG with a non-conformal joining meshes contain 161, 158 and 110 million cells, respectively. Note that only the results with the conforming mesh will be shown in the next sections as the effect on the pressure drop coefficients is negligible (only local effect can be seen on the turbulent kinetic energy for example).

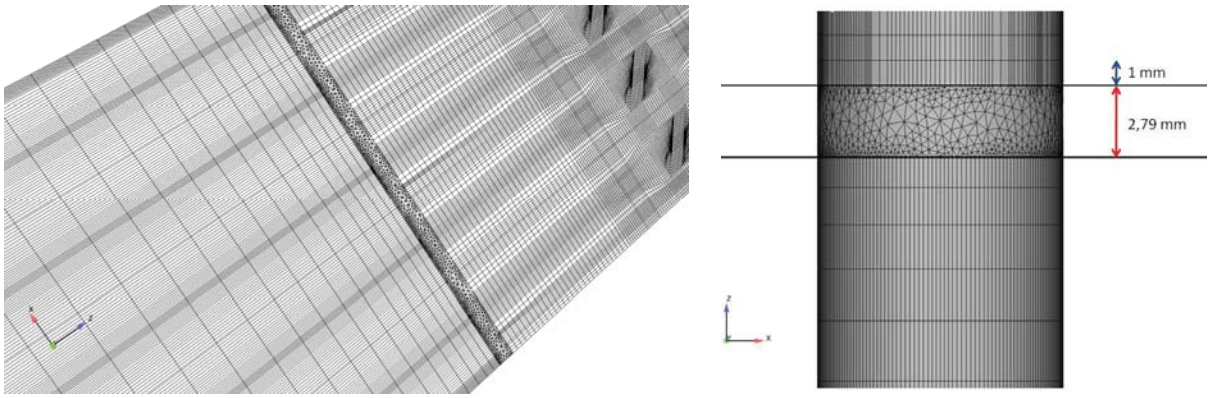

Figure 5 : Conformal joining of the SSG and MVG meshes.

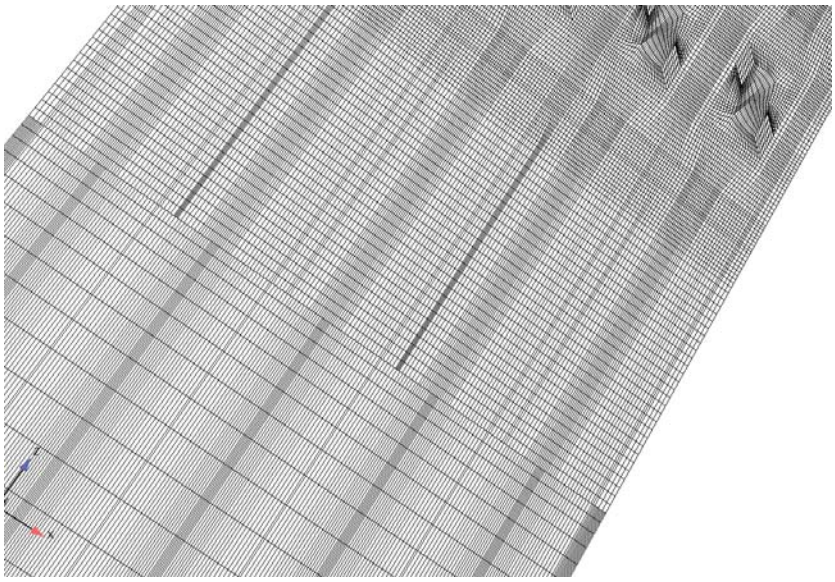

Figure 6 : Non-conformal joining of the SSG and MVG meshes.

3.2 RANS simulations with *Code_Saturne*

Code_Saturne is a highly customisable open source (www.code-saturne.org) CFD package developed by EDF. It is based on a co-located finite volume discretisation and accepts unstructured mesh types with cells of any shape. The velocity and pressure coupling is ensured using the SIMPLEC algorithm. The pressure Poisson equation is solved using an algebraic multigrid method. A Rhie and Chow interpolation method is utilised to reduce oscillatory solutions.

A steady algorithm (which uses a variable time step in space and time) has been used in the present study. This seems *a priori* sufficient as only the steady state is of interest (see section 5 for the effect of the time marching scheme). The convective terms of the momentum equation have been solved using a centered scheme with a slope test which switches to an upwind scheme if the solution in not monotonic. The convective terms of the turbulent quantities have been solved using a pure upwind scheme. Note that the effect of the convection scheme used for the turbulent quantities is negligible in the present study. The gradient computation uses a least square method with an extended neighbourhood for the MVG meshes and an implicit method based on a Gauss integration for the SSG mesh (this mesh is fully conformal and hexahedral and has therefore less skewed cells/faces than the MVG one). Further details on the numerical method utilized in *Code_Saturne* can be found in Archambeau et al. (2004).

Two turbulence models requiring the use of wall functions are utilized (sometimes called High Reynolds Number turbulence models (HRN)), a Linear Eddy Viscosity Model (LEVM), the $k-\epsilon$ model with linear production from Guimet and Laurence [6] and the Speziale Sarkar and Gatski Reynolds Stress Model [7]. Note that the latter is *a priori* more adequate for the complex physics of the flow through tube bundle in particular with the presence of grids equipped with vanes (see Bellet and Benhamadouche [2] in which several swirling flows are studied with different turbulence models).

With the Reynolds Stress Model, 1000 outer iterations (which is enough in the present cases) cost 10 hours with the SSG mesh and 30 hours with the MVG conformal mesh on 2048 cores of EDF BlueGene/P. Note that the number of computational cells is comparable in the two meshes. The computational time is reduced to 8h with the RSM and the non-conformal mesh.

The equations used for each turbulence model are not recalled here for brevity. They can be found in the provided references.

The inlet is a fully developed turbulent flow in both cases, obtained using a 2D periodic computation for the SSG configuration (called periodic bundle in figure 1) and using a periodic computation with one SSG in the MVG configuration (called periodic SSG in figure 2). Note that sensitivity tests have been performed to check the influence of the inlet boundary conditions and that no noticeable effect has been observed on the pressure drop results.

Standard one and two friction velocity scales wall functions are used.
In the standard one friction velocity scale approach, if u_* is the friction velocity at the wall, one solves with a fix point algorithm

$$\begin{cases} \dfrac{U}{u_*} = \dfrac{1}{0{,}42}\ln\left(\dfrac{u_* y}{\nu}\right) + 5{,}2 & \text{if } \; y^+ > y^+_{\text{lim}} \\ \dfrac{U}{u_*} = \dfrac{u_* y}{\nu} & \text{otherwise} \end{cases}$$

where U, y et ν are the tangential velocity at the first near-wall cell, the distance of the first computational cell center to the wall and the kinematic viscosity, respectively. In this case, one imposes $\frac{\partial R_{ii}}{\partial n} = 0$ and $\varepsilon = \frac{u_k^2 u_*}{0{,}42\, y}$ at the wall, where R_{ii} and ε are the diagonal Reynolds stresses (the turbulent kinetic energy k being equal to 0.5 R_{ii}) and the dissipation rate, respectively. In this case, the shear stress at the wall τ_w is equal to $\rho\, u_*^2$, where ρ is the fluid density.

In the standard two friction velocity scales approach, one has

$$\begin{cases} \frac{U}{u_*} = \frac{1}{0{,}42} \ln\left(\frac{u_k y}{\nu}\right) + 5{,}2 \text{ if } y^+ > y^+_{\text{lim}} \\ \frac{U}{u_*} = \frac{u_k y}{\nu} \quad \text{otherwise} \end{cases}$$

with $u_k = C_\mu^{1/4}\sqrt{k}$. In this case, one imposes $\frac{\partial R_{ii}}{\partial n} = 0$ and $\varepsilon = \frac{u_k^3}{0{,}42\, y}$ at the wall. C_μ has a standard value equal to 0.09. In this case, the shear stress at the wall τ_w is equal to $\rho\, u_k u_*$.

Note that sensitivity studies have been performed to check the effect of y^+_{lim} and of the boundary condition applied to the dissipation rate (with one friction velocity scale, $\varepsilon = \frac{u_*^3}{0{,}42\, y}$ or $\varepsilon = \frac{u_k^3}{0{,}42\, y}$, and with two friction velocity scales $\varepsilon = \frac{u_k^2 u_*}{0{,}42\, y}$ have been tested, respectively). The effect was very limited.

Figure 7 shows the time history of the stream-wise velocity at several probes for the MVG configuration with the Reynolds Stress Model combined to a wall function using one friction velocity scale. The present computation has been carried out along 3000 outer iterations but it is clear that the convergence is reached before. The other computations have been limited to 1000 iterations.

The non-dimensional distance of the first computational node to the wall ($y^+ = \frac{u_* y}{\nu}$) is a very important parameter as the present turbulence models are not wall resolved ones (acceptable values should be higher than 15 to 20, 30 to 200 would be ideal). Figure 8 shows this non-dimensional distance along the central rod for the same computation used to show the time histories in figure 7. It is clear that the non-dimensional distances along the bare bundles meshed downstream the MVG and the SSG are not of the same magnitude. The mesh downstream the MVG seems to better fit the requirements (this doesn't mean that the requirements are fulfilled in the MVG or that the mesh is fine enough). As one will see later, tests at higher Reynolds numbers (up to 500000) have been performed (which means that y^+ is globally increased) and the results were of the same quality as those obtained at the present Reynolds number (around 100000).

Note that, unfortunately, due to the cost of the meshing procedure (meshing hexahedral conformal meshes is a very long procedure), no mesh sensitivity study has been performed.

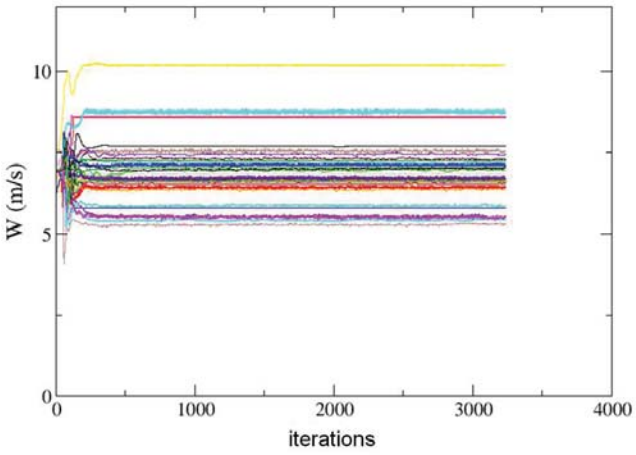

Figure 7 : Time history of the stream-wise velocity at different probes (RSM computation with one friction velocity scale, MVG configuration)

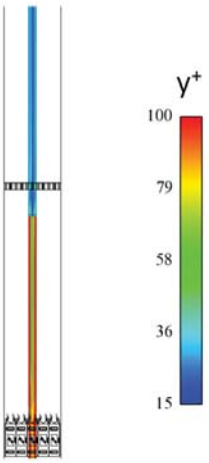

Figure 8 : y^+ one the central rod along two successive spans (RSM computation with one friction velocity scale, MVG configuration)

4 PRESSURE DROP RESULTS

Hereafter, K is the pressure loss coefficient:

$$K = \frac{\Delta p}{\frac{1}{2}\rho U_d^2}$$

Δp is the difference between the mean pressure (average over the 2D plane orthogonal to the rod) at two locations given in the experiment [8] (the two locations surround a SSG or MVG) and U_d is the bulk velocity.

4.1 Simple Support Grid (SSG) results

Table 1 gives the pressure drop coefficients for three computations (two RSM combined to the two different wall functions shown earlier and a LEVM combined to a two friction velocity scales wall function).

DPMi are different pressure drop measurements; see [8] for more details. It is clear that there is a dramatic overall underestimation of the pressure drop coefficients. 35% underestimation for the Reynolds Stress Model combined to a wall functions using one friction velocity scale and for the k-ε model with a linear production combined to a wall function using two friction velocity scales. The Reynolds Stress Model with two friction velocity scales gives worse results, the error being around 40%.

In order to check whether the mesh is not too fine in some regions for the turbulence models utilized in the present work, the Reynolds number is increased. Figure 9 shows the pressure drop coefficient as a function of the Reynolds number compared to available experimental data. Note that only the Reynolds number around 100000 has been studied is the framework of EPRI benchmark [8]. One can see that the decrease is similar to the one obtained in the experiment and that there is no jump in the curve (which would correspond to a different behaviour of the turbulence model).
Note also that using an unsteady algorithm (which was possible as the mesh is conformal and hexahedral) didn't modify the results significantly.

Thus, the pressure drop coefficient is dramatically underestimated (around 35%) for the Simple Support Grid (SSG) configuration (one swill see in the next part that there are serious doubts about the experimental values for the SSG configuration).

Table 1: Pressure drop coefficients obtained from CFD compared to experimental data for the SSG configuration

		RSM with one velocity scale		RSM with two velocity scales		k-ε with two velocity scales	
SSG	Exp.	K	Err. (%)	K	Err. (%)	K	Err. (%)
DPM1	0,96	0,62	-35%	0,57	-41%	0,61	-36%
DPM2	0,96	0,62	-35%	0,57	-41%	0,61	-36%
DPM3	0,93	0,62	-33%	0,57	-39%	0,61	-34%
DPM4	0,96	0,62	-35%	0,57	-41%	0,61	-36%
DPM5	0,94	0,62	-34%	0,57	-39%	0,61	-35%
DPM6	0,92	0,62	-33%	0,57	-38%	0,61	-34%

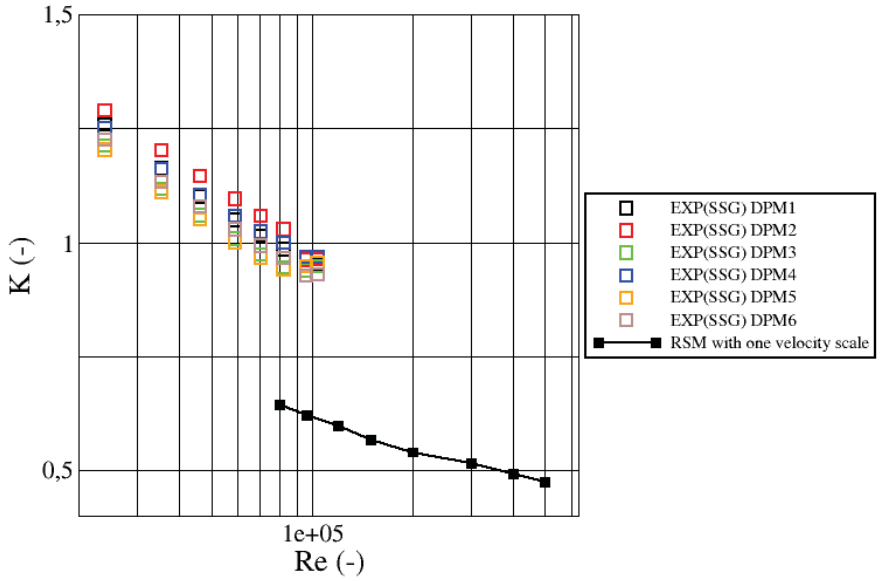

Figure 9: Pressure drop coefficient as a function of the Reynolds number - RSM with one friction velocity scale on the SSG configuration

4.2 Mixing Vanes Grid (MVG) results

Table 2 gives the pressure drop coefficients for three computations (two RSM combined to the two different wall functions shown earlier and a LEVM combined to a one friction velocity scale wall function). k-ε model results combined with a two friction velocity scales wall function are not shown here as they gave comparable results to those obtained with the RSM with the same wall function (slightly better but still far from the results obtained with a one friction velocity scale wall function).

DPMi are different pressure drop measurements; see [8] for more details. The type of the grid is given in the table for every DPMi measurement (the pressure drop coefficient for the bare bundle is measured in MANIVEL experiment between the second and third MVG).

The results with the RSM combined to a one friction velocity scale wall function are first analysed.

The pressure drop along the bare bundle is in perfect agreement with the experimental results. For the two types of grids (SSG and MVG), there is a systematic underestimation of the pressure drop coefficient. The underestimation is comparable for both grids (around. 15%).

This might mean that there is a problem in predicting pure grid turbulence and not the additional pressure drop induced by the vanes. The fact that grid turbulence seems to be under-predicted is confirmed by a deeper analysis performed during the EPRI benchmark for both SSG and MVG (despite a satisfactory prediction of the secondary flow intensity). This underestimation of the turbulent kinetic energy by RANS models has also been observed in KAERI-OECD benchmark in which a split-type mixing grid has been studied [9].

It can also be observed that the measured SSG pressure drop coefficient in the MVG configuration is lower than the one obtained in the SSG configuration. The intuition would lead to the contrary as the Reynolds numbers are almost the same in the two configurations. As the flow is more disturbed by a MVG upstream a SSG than by a SSG upstream a SSG, the secondary flows should be stronger, thus the wall friction should be higher and then the pressure drop should increase. This intuition is confirmed by CFD (the SSG pressure drop coefficient obtained by CFD is higher in the MVG than in the SSG one for comparable Reynolds numbers). This leads to some doubts about the experimental results for the SSG configuration. If one believes that the global tendencies are well predicted by CFD computations (SSG pressure drop coefficient around 0.68 in the MVG configuration and around 0.62 in the SSG configuration) and considers that the experimental results are right in the MVG configuration (pressure drop coefficient around 0.8), applying the CFD factor (0,62/0,68) leads to an estimated experimental SSG pressure drop coefficient of 0.72, rather than a value around 0.95 as predicted by the experiment in the SSG configuration (the real value should be a bit lower).

The tendency is the same for the two other computations with an overall underestimation. However, one can notice that the use of a two friction velocity scales wall function worsens the results. The pressure drop coefficients obtained with the k-ε model with a linear production are slightly better than those obtained with the RSM (the underestimation is rather around 11% for both grids). There is no explanation for this up to now except the fact that the wall functions have been developed and intensively tested for the standard k-ε model and directly transposed to the RSM.

In order to check whether the mesh is not too fine in some regions (at least in the bare bundles, the mesh being too complex in the MVG) for the turbulence models utilized in the present work, the Reynolds number is increased. Figure 10 shows the pressure drop coefficient as a function of the Reynolds number compared to available experimental data. Note that only the Reynolds number around 100000 was studied is the framework of EPRI benchmark [8]. One can see that the decrease is similar to the one obtained in the experiment for all the pressure drop coefficients (bare bundle, SSG and MVG ones) and that there is no jump in the curve (which would correspond to a different behaviour of the turbulence model).
Thus, the pressure drop coefficient is strongly underestimated (around 15% with the best computation for the Simple Support Grid (SSG) and for the Mixing Vane Grid (MVG)) in the MVG configuration. The bare bundle pressure drop coefficient is almost perfectly predicted (around 1% error).

Table 2: Pressure drop coefficients obtained from CFD compared to experimental data for the MVG configuration

		RSM with one velocity scale		RSM with two velocity scales		k-ε with two velocity scales	
SSG	Exp	K	Err. (%)	K	Err. (%)	K	Err. (%)
DPM1 (MVG)	1,63	1,36	-16%	1,01	-38%	1,41	-13%
DPM2 (bare bundle)	0,57	0,57	1%	0,39	-32%	0,58	2%
DPM3 (MVG)	1,61	1,39	-13%	0,99	-38%	1,44	-10%
DPM4 (SSG)	0,81	0,68	-17%	0,52	-36%	0,71	-13%
DPM5 (MVG)	1,62	1,39	-14%	0,99	-39%	1,44	-11%
DPM6 (SSG)	0,78	0,68	-13%	0,52	-33%	0,71	-9%

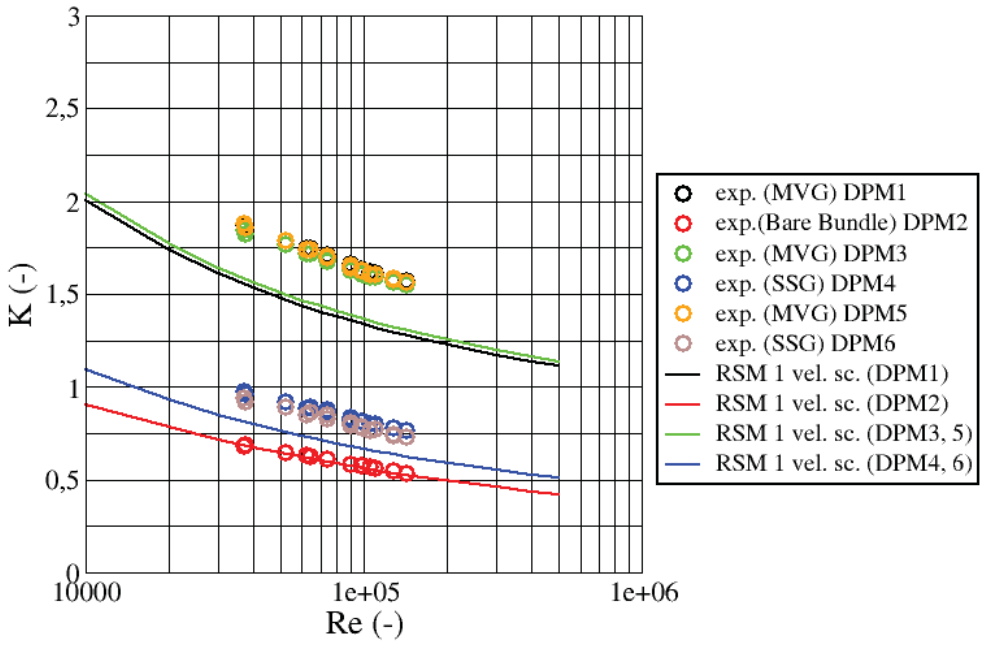

Figure 10 : Pressure drop coefficient as a function of the Reynolds number - RSM with one friction velocity scale on the MVG configuration

5 SENSITIVITY STUDY WITH ONE MVG

The non-conformal or conformal joinings which have been forced by the different topologies of the SSG and MVG didn't allow us to use the recommended (default) options in *Code_Saturne*. The gradient computation was ensured using a least square method which is known to be less accurate than the implicit computation using Gauss integration. Moreover, the unsteady algorithm was not usable as well. In order to test the effect of these two numerical options, one

isolates the MVG and its corresponding bundles upstream and downstream and performs computation on a fully hexahedral and conforming mesh.

The computational domain which has been studied here in represented in figure 11. The inlet conditions are fully developed[1]. The different cases are summarized in table 3. The turbulence model which has been used is the Reynolds Stress Model which has been used previously. The wall functions are the standard ones using one friction velocity scale[2]. The convection scheme is the standard one using a fully centered scheme with a slope test for the velocity components and a full 1st order upwind scheme for the turbulent quantities[3]. Only the time advancing scheme (steady or unsteady 1st order Euler) and the computation of the gradients (Least Squares[4] and Gauss) are changed. Figure 12 gives the evolution of the mean pressure along the stream-wise direction.

Neither using the Gauss method to compute the gradients but with a steady algorithm (case 1) nor the unsteady algorithm with a Least square method (case 2) improve the results that much. However, combining both the Gauss and the unsteady algorithms (case 3) impressively improves the pressure drop prediction. This clearly shows the importance of the numerical approach with the present mesh (fully conformal hexahedral mesh). Note that the turbulent kinetic energy seems to be still low.

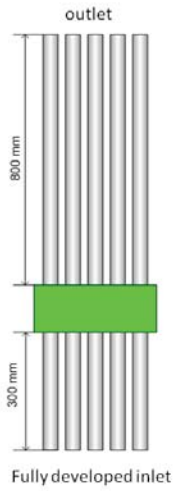

Figure 11: The reduced computation domain

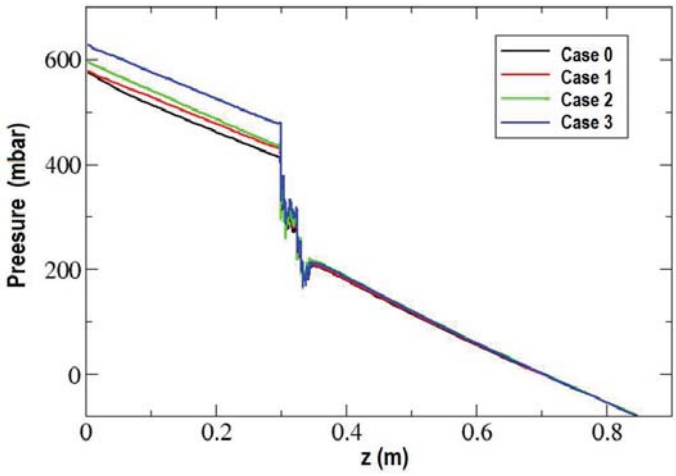

Figure 12: Mean pressure evolution along the computational domain

[1] The use of constant inlet boundary conditions has no impact on the pressure drop as the upstream bare rod bundle in long enough.

[2] Note that using a standard wall function with two velocity scales with the options of case 3 deteriorates the results.

[3] Note that the use of a centered scheme with a slope test for the turbulent quantities doesn't change the results of case 3.

[4] This scheme has been used in all the computations using the RSM in the present article for the MVG configuration.

Table 3: Pressure loss dependence on the numerical options

	Algorithm	Gradients	pressure loss (mbar)
Case 0	Steady	Least square	317
Case 1	Steady	Gauss	331
Case 2	Unsteady	Least square	335
Case 3	Unsteady	Gauss	372
Experimental Average	-	-	373

6 CONCLUSIONS

Two types of grids, a simple (SSG) and a complex (MVG) one, have been studied at a Reynolds number around 100000 with a focus on the pressure drop coefficient. Both a first and a second moment closure RANS turbulence model have been utilized. Two wall functions have also been tested.
The effect of the turbulence model is, for the pressure drop prediction, negligible compared to the influence of the wall function. The standard wall function using one friction velocity, although not suitable in other configurations, gives the best results.
A systematic underestimation of the pressure drop is obtained for the SSG (around 15% for the best results) even with the best numerical options, usable as the mesh is fully conformal and hexahedral. A systematic underestimation is also observed for the MVG (around 15% error) but with deteriorated numerical options (a steady algorithm and a least square method for computing the gradients) forced by the mesh complexity with alternating SSGs and MVGs (the mesh is fully hexahedral by parts and either a conformal joining using tets/pyramids or a non-conformal joining are used to link SSG and MVG meshes).
Additional tests have been carried out with just one MVG and allowed us to test the effect of the time scheme and the gradient computation. The use of an unsteady algorithm combined to a Gauss implicit gradient computation improved the CFD predictions.

7 ACKNOWLEDGMENTS

The author would like to acknowledge all the participants to the Round Robin exercise organized by EPRI around CEA-EDF-EPRI Nestor project.

8 REFERENCES

1. F. Archambeau, N. Mechitoua, and M. Sakiz, “Code_Saturne: A finite volume method for the computation of turbulent incompressible flows: Industrial applications,” *International Journal on Finite Volumes*, **1**(1) (2004).
2. S. Bellet & S. Benhamadouche, "Impact of rotating and secondary flows on PWR primary loops, CFD might bring some light on the flow behavior", *Icone 18, Xi’an, China, May 2010*.
3. Bergeron, A., Chataing, T., Décossin, E., Garnier, J., Péturaud, P., Yagnik, S.K., 2007, “Design, Feasibility, and Testing of Instrumented Rod Bundles to Improve Heat Transfer Knowledge in PWR Fuel Assemblies”, International LWR Fuel Performance Meeting, San Francisco, September 30-October 3, 2007.

4. L. Capone. Private communication (2012).
5. Conner, M.E., Baglietto, E., Elmahdi, A.M., "CFD Methodology and Validation for Single-Phase Flow in PWR Fuel Assemblies," Nuclear Engineering and Design, Vol. 240, pp. 2088-2095, (2010).
6. V. Guimet and D. Laurence, "A linearised turbulent production in the k− ε model for engineering applications," *Proceedings of the 5th International Symposium on Engineering Turbulence Modelling and Measurements*, Mallorca, Spain (2002).
7. C. G. Speziale, S. Sarkar and T.B. Gatski, "Modelling the pressure–strain correlation of turbulence: an invariant dynamical systems approach," *Journal of Fluid Mechanics*, **227**, pp. 245-272 (1991).
8. D. Wells and Y. Hassan, "Overview of CFD Round Robin Benchmark of the High Fidelity Fuel Rod Bundle NESTOR Experimental Data", The 16th International Topical Meeting on Nuclear Reactor Thermal Hydraulics (NURETH-16) , Hyatt Regency Chicago, Chicago, IL, USA, August 30-September 4 (2015).
9. J.R. Lee, J. Kim and C-H. Song "Synthesis of the turbulent mixing in a rod bundle with vaned spacergrids based on the OECD-KAERI CFD benchmark exercise", Nuclear Engineering and Design 279 3–18 (2014).